Sensor Layout Design for Structural Health Monitoring

JungHyun Kyung [1], Jae-Hyoung An [1], Hee-Chang Eun [1*]

[1] Department of Architectural Engineering, Kangwon National University, Chuncheon 24341, Republic of Korea.

Abstract

This study investigates the enhancement of optimal sensor placement (OSP) algorithms by incorporating modal reduction constraints and developing combined techniques. The primary goal is to optimize sensor placement for structural health monitoring (SHM), thereby improving the efficiency of information acquisition within practical constraints. The proposed methodology utilizes iterative elimination and combined criteria to evaluate various sensor configurations. Numerical experiments demonstrate distinct sensor layouts derived from diverse algorithmic approaches. The study's novel contributions include the integration of modal strain energy, effective independence (EI), and modal assurance criterion (MAC) techniques into a unified framework, enhancing adaptability to a wide range of SHM scenarios.

Keywords: Optimal Sensor Placement; Fisher Information Matrix; Effective Independence; Modal Reduction; Modal Strain Energy; Combined Approach.

1. Introduction

Structural health monitoring (SHM) is a technique used to assess structural performance by measuring and analyzing responses to external and environmental excitations. Advances in measurement technology, including the development of sensitive sensors, have facilitated the emergence of various SHM techniques, which have been extensively applied to numerous structures. The primary objective of optimal sensor placement (OSP) is to strategically design a subset of candidate positions for measurement sensors. Due to practical limitations, such as cost constraints, OSP schemes employing a limited number of sensors have been rigorously investigated [1-6].

Most existing OSP algorithms utilize iterative methods to exclude degrees of freedom (DOFs) with minimal contributions to the objective function's signal strength from the candidate sensor locations. These algorithms iteratively eliminate sensor positions with the least contribution to linear independence until the target number of sensors is attained. Various objective functions and analytical approaches, such as maximizing the determinant of the Fisher information matrix (FIM) or minimizing the sum of off-diagonal elements in the modal assurance criterion (MAC), are commonly employed in these methods. In practical applications, three variants of FIM—minimum singular value, determinant, and trace—are frequently used to optimize information acquisition and reduce parameter estimation uncertainties. Researchers have also introduced multi-objective optimization schemes for sensor placement, utilizing methods such as mode-shape interpolation and artificial bee colony algorithms. For instance, Gomes et al. [7] proposed a multi-objective sensor location optimization approach using FIM and mode-shape interpolation methods, while Sun & Buyukozturk [8] introduced a discrete optimization scheme based on an artificial bee colony algorithm and MAC-oriented objective functions.

Among OSP techniques, the effective independence (EI) method proposed by Kammer [9] has been widely adopted for maximizing the determination of FIM. This technique evaluates the information efficiency of a sensor array by employing FIM to measure the amount of information collected from sensors. The EI method iteratively optimizes sensor positions by excluding rows of the diagonal elements in the EI matrix with the lowest signal strength at each step, ultimately positioning sensors at nodes with high EI values. Friswell and Castro-Triguero [10] explored the linear independence and signal strength of target modes in the EI method. Considering uncertainties in OSP algorithms, Castro-Triguero et al. [11] compared sensor-layout designs, while Gonen et al. [12] examined the robustness of the EI method under structural uncertainties.

The Guyan reduction technique has been shown to enhance OSP designs under specific conditions. Penny et al. [13] discussed two methods for Guyan reduction and FIM-based OSP approaches. Lu et al. [14] developed an OSP algorithm integrating a genetic algorithm, the Guyan reduction method, and a structural subsection approach. Mercer et al. [15] [9] compared various reduction methods, including Guyan reduction and equivalent reduction expansion processes. The MAC technique identifies optimal sensor layouts by comparing analytical and experimental mode shapes. It aims to design sensor layouts that maximize the off-diagonal elements of the MAC matrix. He et al. [16] introduced an improved adaptive genetic algorithm (IAGA) combined with a modified modal assurance criterion (MMAC) to address issues such as low modal energy and extended computation times. Fu & Yu [17] proposed an OSP scheme incorporating a mathematical MAC and single parenthood genetic algorithm (SPGA). Brehm et al. [18] enhanced the conventional MAC algorithm by introducing physical information into the numerical model. Coote et al. [19] compared existing OSP algorithms for helicopter fuselage measurements.

The placement of sensors often considers the distribution of modal strain energy (MSE), which effectively captures a system's modal characteristics by locating sensors in areas with high MSE. MSE is a sensitive damage indicator and has been widely used for structural damage detection [20-24]. Zhang et al. [25] proposed an OSP scheme based on information gain and modal expansion methods within a Bayesian framework. Liu et al. [26] introduced an improved genetic algorithm for OSP using MSE and MAC. Other researchers, such as Zheng et al. [27], combined MSE with graph theory for optimal matching in sensor placements. Additionally, Seyedpoor et al. [28] developed a damage detection method using OSP and MSE indices, while Salama et al. [29] evaluated candidate sensor locations based on modal kinetic energy (MKE). Li et al. [30] explored the relationship between MKE and EI techniques.

Hybrid OSP techniques combine multiple criteria to achieve comprehensive and efficient sensor configurations. For instance, Chen et al. [1] employed an energy revision factor to measure MSE and proposed a hybrid OSP algorithm combining MAC and EI techniques. He et al. [16] introduced an OSP method integrating a modified MMAC and an improved adaptive genetic algorithm to address limitations of the traditional MAC approach.

Recent advancements in SHM methodologies have highlighted the importance of optimizing sensor layouts to maximize information efficiency under cost and resource constraints. Despite significant progress, challenges remain in balancing computational efficiency and real-world applicability. This study addresses these gaps by proposing modified and hybrid OSP techniques. Recent studies emphasize the need for algorithms adaptable to diverse structural environments, yet comprehensive comparisons and practical implementations are limited [31-37]. By integrating MSE, EI, and MAC techniques, this research contributes a novel framework for efficient sensor placement.

This study effectively addresses challenges in sensor layout design by introducing robust, iterative, and hybrid approaches that enhance the accuracy and adaptability of sensor placements. These results are highly applicable to a wide range of SHM applications, providing a strong foundation for further innovations in monitoring infrastructure. Preliminary sensors are typically designed using reduced models retained through methods such as the Guyan condensation technique or modal reduction constraints. The dynamic system can be condensed using these constraints and subsequently expanded to a full set of DOFs. The proposed methods iteratively move DOFs with low independence in master locations to slave DOFs, determining final sensor placements based on high signal strength and independence. The validity and comparative performance of the proposed methods are illustrated through a numerical example, revealing that inconsistencies in sensor layouts stem from differences in objective functions and analytical processes. This study concludes that sensor design should align with the specific measurement purpose, as summarized in Figure 1, which outlines the research flow for deriving and applying optimal sensor design algorithms from measured data.
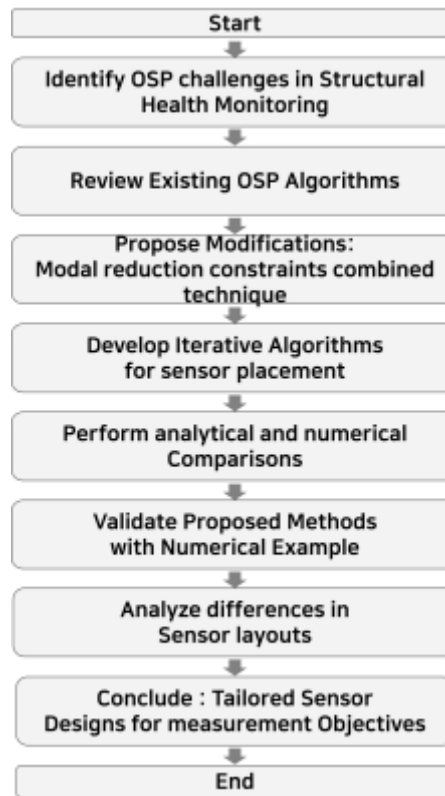
Figure 1. Research flowchart

2. Modification of Existing OSP Algorithms

Most OSP algorithms are derived from the modal analysis of a structural finite element model and employ iterative schemes to determine the optimal sensor layout. The algorithms identify the final sensor layout by excluding coordinates that exhibit the lowest independence from the objective function at each iteration. The effects of the excluded DOFs can be ignored in subsequent iterations or retained for consideration. In this study, the removed mode shapes affect the following iterations through modal constraints, and the OSP algorithms identify the locations with high signal strength.

This section introduces OSP algorithms designed to determine l target sensor positions from an initial set of n candidate sensor locations ($l \leq n$) of the reduced analytical model while satisfying the constraint conditions. Initially, the candidate sensor locations correspond to the entire DOF n of the analytical model. Modal constraints are expressed as a relationship between master and slave DOFs. This study proposes modified OSP algorithms, applying the FIM obtained through data expansion and modal reduction using constraints from the condensed modal matrix coefficients to the EI algorithm. This section also introduces modified forms of the MSE and MAC methods using modal reduction constraints, as well as a combined technique that integrates these two methods. The validity of the proposed methods is illustrated through analytical and numerical comparisons.

2.1. Modal Reduction-based EI Approach

2.1.1. Modal Reduction

The constraints of the reduced modal matrix, mediated by master and slave modal matrices between generalized coordinates and modal coordinates, are established. Sensor positions are predicted by minimizing the covariance matrix of the response estimation error. The dynamic equation for an analytical model with n DOFs (without damping) can be expressed as:

$$M\ddot{x} + Kx = 0 \tag{1}$$

where M and K denote the $n \times n$ positive-definite mass and stiffness matrices, respectively, and $\mathbf{x}(t)$ represents the $n \times 1$ displacement vector. The initial candidate sensor locations correspond to the entire DOF of the system. Since modal characteristics directly relate to dynamic responses, sensor positions are derived from modal analysis.

The generalized and modal displacement vectors have the following relationship:

$$x(t) = \phi q(t) \tag{2}$$

where ϕ represents the $n \times r$ incomplete target mode shape matrix corresponding to the lowest r modes and $q(t)$ is the $r \times 1$ modal displacement vector. The number of considered mode shape vectors r must be less than or equal to the number of target sensors l.

Dividing the generalized coordinates into master and slave coordinates yields:

$$x_m = \phi_m q(t) \text{ and } x_s = \phi_s q(t) \tag{3}$$

here, ϕ_m and ϕ_s represent the $(n - v) \times r$ master and $v \times r$ slave mode shape matrices, respectively. The $(n - v)$ master coordinates correspond to candidate sensor locations, while the v slave coordinates are excluded from the candidate sensor positions. The candidate sensor locations are initially set equal to the entire DOFs, and the DOFs with expected low signal strength are excluded at each iteration step.

In the first attempt, to start, the candidate sensor locations are set equal to $n - 1$, excluding the DOF where signal strength is expected to be low. The slave coordinates increase by one after each iteration, whereas the master decreases by one. This process is repeated until the master DOFs match the number of target sensors. The modal data that moves to the slave DOFs is used in the next iteration of the reduced model using Equation 3.

Constraint conditions were generated by reducing the mode shape matrix to the master DOFs, and these constraints were used to modify the existing OSP techniques. By solving the first Equations in Equation 3 with respect to the modal coordinate vector $q(t)$ with the help of the generalized inverse, we obtain

$$q(t) = \phi_m^+ x_m \tag{4}$$

where the superscript "+" indicates the Moore-Penrose inverse. Substituting Equation 4 into the second equation of Equation 3 yields the following relationship between the master and slave displacement vectors:

$$x_s = \phi_s \phi_m^+ x_m \tag{5a}$$

$$x = \begin{bmatrix} x_m \\ x_s \end{bmatrix} = T x_m \tag{5b}$$

where, $T = \begin{bmatrix} I \\ \phi_s \phi_m^+ \end{bmatrix}$ and I is the $(n - v) \times (n - v)$ identity matrix, and v denotes the number of slave DOFs excluded from the total DOFs. Equation (5a) represents the constraint condition for establishing the relationship between the master and slave coordinates of the target modes in each iteration. It is observed that the displacement vector of the entire DOFs of the dynamic system is condensed only by the master DOFs.

The observation responses including external white noise at measurement from Equation 5b can be expressed by:

$$x(t) = T x_m + \xi(t) \tag{6}$$

where $\xi(t)$ is the $n \times 1$ Gaussian white noise vector.

The observation displacement vector, x_m, can be expressed by

$$x_m = T^+ \big(x(t) - \xi(t) \big) \tag{7}$$

The unbiased estimated displacement vector corresponding to the master DOFs $\hat{x}_m$, is written as:

$$\hat{x}_m = T^+ x(t) \tag{8}$$

Equations 7 and 8 represent the values necessary for estimating the covariance matrix of the displacement response estimation error, which we denote as the method M-1.

2.1.2. Constrained Modal Reduction

This technique estimates the displacement vector corresponding to the entire DOFs using the incomplete mode shape matrix and the constraints written as:

$$\begin{bmatrix} \phi_s \phi_m^+ & -I \end{bmatrix} \begin{bmatrix} x_m \\ x_s \end{bmatrix} = 0 \tag{9}$$

The displacement vector is estimated by iteratively adjusting master DOFs using a least-squares approach. This process minimizes the difference between the analytical displacement vector and the displacement vector obtained from

the incomplete mode shape matrix. Letting matrix A be the coefficient matrix in Equation 9, it can be expressed in matrix form as:

$$Ax = 0 \tag{10}$$

where $A = [\phi_s\phi_m^+ \quad -I_{v\times v}]$ and $x = \begin{bmatrix} x_m \\ x_s \end{bmatrix}$. Solving Equation 10 with respect to the displacement vector by the solution of the linear Equations using Moore-Penrose inverse, it yields

$$x = (I - A^+A)h \tag{11}$$

where h is an $n \times 1$ arbitrary vector.

The objective function of the difference between two displacement vectors is established as follows:

$$P = (x - x_a)^T(x - x_a) \tag{12}$$

where x_a represents the analytical displacement vector obtained using the full mode shape matrix of the analytical model, while x denotes the displacement vector to be estimated.

The displacement vector of the entire DOFs is estimated by determining an arbitrary vector h. This is achieved by minimizing the performance index based on the least-squares approach. By substituting Equation 11 into Equation 12 and considering the minimization condition, we obtain

$$h = (I - A^+A)x_a + A^+Ag \tag{13}$$

where g denotes an $n \times 1$ arbitrary vector. Substituting Equation 13 into Equation 11, it gives

$$x = (I - A^+A)x_a \tag{14}$$

where $(I - A^+A)^T = I - A^+A$ and $A^+AA^+ = A^+$. Equation 14 expresses the displacement vector to be expanded to a full set of DOFs. Since Equation 14 represents the displacement-based relationship, the corresponding relationship based on acceleration would be as follows:

$$\ddot{x} = (I - A^+A)\ddot{x}_a \tag{15}$$

Equation 15 corresponds with the constrained motion Equation proposed by Udwadia and Kalaba, yielding the same result as assuming the weight matrix as the identity matrix instead of the mass matrix.

Equation 14 in terms of the displacement vector corresponding to the master DOFs can be expressed by

$$x_m = B_1x = B_1(I - A^+A)x_a \tag{16}$$

where B_1 denotes the $(n - v) \times n$ Boolean matrix specifying the master DOFs. The biased and unbiased displacement vectors can be expressed, respectively, by

$$x_m = B_1(I - A^+A)(x_a + \gamma) \tag{17}$$

$$\hat{x}_m = B_1(I - A^+A)x_a \tag{18}$$

Similarly, utilizing Equations 17 and 18 as in M-1, we denote it as the method M-2.

2.1.3. Modal Reduction-based EI Approach

In previous sections, two methods (M-1 and M-2) were introduced to estimate biased and unbiased displacement vectors. Estimation accuracy is evaluated by mean square error, which measures the average squared difference between the true parameter and its estimate. The covariance matrix of the displacement response estimation error for the M-1 method can be expressed as:

$$Cov(\hat{x}) = FIM^{-1}\sigma^2 \tag{19}$$

where FIM denotes the Fisher information matrix, and σ^2 represents the stationary Gaussian white variance matrix. Similarly, the covariance matrix for the M-2 method can be expressed by substituting relevant values into the above Equation.

The EI algorithm designs an optimal sensor layout by selecting positions that correspond to the maximum FIM. If a small FIM indicates low independence, the corresponding master DOF is moved to a slave DOF, and the coefficient matrices are updated in subsequent iterations. This process continues until the desired number of sensors is obtained. Thus, the covariance matrix of the displacement response estimation error of the M-1 in section 2.1.1 can be expressed as follows:

$$J = E[(x_m - \hat{x}_m)(x_m - \hat{x}_m)^T] = \left(\hat{T}^+\xi(t)\right)\left(\hat{T}^+\xi(t)\right)^T = \left(\frac{1}{\xi(t)\xi(t)^T}\right)^+ \left(\hat{T}^T\hat{T}\right)^+ \tag{20}$$

where $\hat{T} = B_1 T$. $\hat{T}^T\hat{T}$ is the $(n - v) \times (n - v)$ FIM utilized as an objective function to estimate the OSP. $\xi(t)$ is the $(n - v) \times 1$ Gaussian white noise vector and $\frac{1}{\xi(t)\xi(t)^T}$ represents the stationary Gaussian white variance matrix.

Similarly, the covariance function using the displacement vectors of the M-2 in section 2.1.2 can be written by

$$J = E[(x_m - \hat{x}_m)(x_m - \hat{x}_m)^T] = \left(R^+\gamma(t)\right)\left(R^+\gamma(t)\right)^T = \left(\frac{1}{\gamma(t)\gamma(t)^T}\right)^+ (R^T R)^+ \tag{21}$$

where $R^T R$ represents the $(n - v) \times (n - v)$ FIM and $R = B_1(I - A^+ A)$, $\gamma(t)$ is the $(n - v) \times 1$ Gaussian white noise vector and $\frac{1}{\gamma(t)\gamma(t)^T}$ represents the stationary Gaussian white variance matrix.

It is observed in Equations 20 and 21 that the objective function J is minimized at the maximum FIM. This indicates that the observed and estimated displacement vectors nearly coincide at the maximum FIM. The EI algorithm designs the optimal sensor layout at positions corresponding to the maximum FIM. If a small FIM exhibits low independence from the OSP, the corresponding master DOF moves to the slave DOF, and the coefficient matrices $\hat{T}$ and R are recalculated for the next iteration. The master DOFs in the iteration process are continuously selected and moved to the slave DOFs, and the final l $(l \geq r)$ optimal positions are ultimately obtained at the end of the repeated process.

The mode shapes are linearly independent, and the EI algorithm designs the sensors at positions that represent the high independence of the mode-shape matrix. The EI distribution matrix of the candidate sensors, E_E, provided by Kammer [10] can be expressed as:

$$E_{E1} = [\hat{T}\eta_1]\otimes[\hat{T}\eta_1]\lambda_1^{-1}\{1\} \tag{22a}$$

or;

$$E_{E2} = [R\eta_2]\otimes[R\eta_2]\lambda_2^{-1}\{1\} \tag{22b}$$

where λ_i and η_i $(i = 1,2)$ represent the eigenvalue and the corresponding eigenvector of the $(n - v) \times (n - v)$ FIMs, $\hat{T}^T\hat{T}$ and $R^T R$, respectively. The vector η_i $(i = 1,2)$ is orthogonal, $\{1\}$ is a $(n - v) \times 1$ column vector with all elements of 1, and $\otimes$ represents the term-by-term matrix multiplication. The subscripts 1 and 2 correspond to the methods M-1 and M-2, respectively. Equation (22b) represents the EI distribution matrix corresponding to the master DOFs in the method M-2.

It can be observed that the sensor layout design is sensitive to the signal strength related to the eigenvalue of the FIM. The contribution of sensor placement to spatial independence can be evaluated using the EI matrices E_{Ei} $(i = 1, 2)$. The DOF with the smallest EI, which represents the lowest independence among the master DOFs of Eq. (22b), is moved to the slave location.

Alternatively, EI can be calculated using the diagonal of E_D as follows: From the properties of the eigenvalue and eigenvector of the FIM, $\eta_1^T\hat{T}^T\hat{T}\eta_1 = \lambda_1$, $\eta_2^T R^T R\eta_2 = \lambda_2$, and $\eta_i^T\eta_i = I$ $(i = 1,2)$, the EIs on the M-1 and M-2 can also be written by:

$$E_{D1} = diag\{\hat{T}\eta_1\lambda^{-1}\eta_1^T\hat{T}^T\} \tag{23a}$$

$$E_{D2} = diag\{R\eta_2\lambda_2^{-1}\eta_2^T R^T\} \tag{23b}$$

Matrix E_D is an orthogonal projection and idempotent matrix, and its trace corresponds to its rank. The E_D indices in Equations 23 represent the contribution of the sensor locations.

Equations 23 are another forms of Equations 22a and 22b for the EI scheme. In each iteration, the coefficient matrix of Equations 23 is re-established. The master DOF of the smallest E_D index is moved to the slave sensor location, and the same process is repeated until the sensor number reaches the target number.

2.2. Static Condensation-based Modal Energy Techniques

The static condensation method reduces the size of a system by eliminating slave DOFs. Modal energies such as MSE and MKE are used as indices for OSP. MSE is expressed as a function of the stiffness and mode shape matrices and is sensitive to structural damage, making it a valuable metric for sensor placement. The MSE is sensitive to structural damage because the modal strain is closely related to the dynamic characteristics of a structure. The structural MSE of the overall structural stiffness matrix in mode i can be written as follows:

$$MSE_i = \frac{1}{2}\phi_i^T K \phi_i \tag{24}$$

where ϕ_i denotes the ith normalized mode shape vector, and K is the stiffness matrix. The MSE of the jth element for the ith order mode can be expressed as:

$$MSE_{ij} = \frac{1}{2}\phi_i^T K_j \phi_i \tag{25}$$

This modified MSE (MMSE) tracks the OSP using the modal strain energy, which is determined by the reduced stiffness matrix and the corresponding reduced mode shape matrix, in terms of master DOFs. The master DOFs with low indices in the objective function are moved to slave DOFs, and static condensation technique is performed. The MMSE technique is obtained by multiplying the condensed stiffness matrix corresponding to the master DOFs with the reduced mode shape matrix. This MMSE is used to re-establish the condensed objective function in each iteration. By substituting Equation 4 into the first equation of Equation 3, a relationship involving only the master DOFs is utilized:

$$x_m = \phi_m \phi^+ q \tag{26}$$

The stiffness matrix is condensed into master DOFs using Guyan's static condensation method. The static equilibrium equation can be written by:

$$Kx=F \tag{27}$$

where the stiffness matrix K can be partitioned into four submatrices:

$$K = \begin{bmatrix} K_{mm} & K_{ms} \\ K_{sm} & K_{ss} \end{bmatrix} \tag{28}$$

where K_{mm} corresponds to $(n-v)$ master DOFs, K_{ss} v slave DOFs, and K_{ms} and K_{sm} are the coupling terms between master and slave DOFs. And $x = [x_m^T \quad x_s^T]^T$ and $F = [F_m^T \quad F_s^T]^T$. Assuming that the forces on the slave DOFs are negligible and solving for the slave displacement x_s, it leads to:

$$x_s = -K_{ss}^{-1}K_{sm}x_m \tag{29}$$

where x_m represents the master displacement vector. Inserting x_s in the first equilibrium equation of Equation 27, it yields:

$$(K_{mm} - K_{ms}K_{ss}^{-1}K_{sm})x_m = F_m \tag{30}$$

where F_m represents the master force vector. The $(n-v) \times (n-v)$ condensed stiffness matrix K_{red} is written by

$$K_{red} = K_{mm} - K_{ms}K_{ss}^{-1}K_{sm} \tag{31}$$

The MMSE can be written by:

$$MMSE = \frac{1}{2}LG^T K_{red}GL^T \tag{32}$$

where $G]_{(n-v)\times n} = \phi_m \phi^+$ and L denotes an $(n-v) \times n$ Boolean matrix to define the candidate sensor locations or master DOFs. The objective function effectively reduces the computational complexity by focusing on the master DOFs and incorporating the effects of the slave DOFs through the condensation process.

Multiplying and summing the ith row of the MMSE matrix and its transpose, and taking the results of the square root gives:

$$MMSE_i = \sqrt{\sum_{j=1}^{n-v} MMSE_{ij} \times MMSE_{ji}} \ , i = 1,2,\ldots,n-v \tag{33}$$

The candidate sensor positions corresponding to the lowest MMSE indices are moved to the slave DOFs, and the coefficient matrix G is updated. A similar process is repeated until the candidate sensor positions correspond with the number of target sensors.

If weighting matrix K in Equation 24 is replaced by mass matrix M, which is the MKE, we obtain:

$$MKE_{ij} = \frac{1}{2}\phi_i{}^T M_j \phi_i \tag{34}$$

Since the mode shapes are orthogonal with respect to the mass matrix, the mass matrix in Equation 34 can be assumed to be an identity matrix. The result takes the same form as the FIM in Equation 20 based on the mode shapes, and the identical OSP results can be estimated.

2.3. MMAC

The MAC is a statistical measure used to quantify the degree of consistency between mode shapes obtained from different sources, such as experimental data and analytical models. MAC values range from 0 to 1, indicating the correlation between two mode shapes. A MAC value close to 1 signifies a high degree of correlation, while a value close to 0 indicates low or no correlation. Mathematically, MAC is defined as:

$$MAC(\phi_i, \phi_j) = \frac{\left|\phi_i^T \phi_j\right|^2}{\left(\phi_i^T \phi_i\right)\left(\phi_j^T \phi_j\right)} \tag{35}$$

where ϕ_i and ϕ_j denote the *i*-th and *j*-th mode shapes, respectively. The numerator in the equation represents the squared magnitude of the inner product of ϕ_i and ϕ_j, while the denominator is the product of their norms.

For OSP, MAC is computed using the reduced mode shape matrix corresponding to the master DOFs, rather than considering all DOFs. A modified version of MAC, denoted as MMAC, is derived for OSP using the same process but focused on the reduced model. The MMAC technique is derived for the OSP:

$$MMAC(G_i, G_j) = \frac{\left|G_i^T G_j\right|^2}{\left(G_i^T G_i\right)\left(G_j^T G_j\right)} \tag{36}$$

In this method, the master DOFs with low signal strength are moved to the slave coordinates iteratively until the desired sensor layout is achieved.

2.4. Combined Approaches (CA)

In practical applications, it is often beneficial to integrate multiple OSP techniques to achieve a comprehensive and effective sensor configuration. CA merge techniques like MMSE and MMAC to consider both modal strain energy and modal consistency. The objective is to create a sensor layout that maximizes both criteria, allowing for flexibility in prioritizing one objective over the other based on specific structural analysis requirements.

The combined optimization objective is formulated as the product of normalized MMSE and MMAC values for each mode shape, defined as:

$$J_i = \lambda \cdot MMSE_i + (1 - \lambda) \cdot MMAC_i \tag{37}$$

where J_i is the combined objective function for the *i*-th sensor location and λ is a scalar coefficient that balances the contribution of MMSE and MMAC. By adjusting λ, the weighting of each criterion can be tuned based on the measurement goals. The iteration process follows the same procedure as in the MMSE and MMAC techniques, ultimately resulting in an optimal sensor placement.

3. Numerical Example

The proposed modifications to the OSP techniques and their CA were validated using a numerical example involving a simply supported truss structure. Figure 2 depicts the truss structure and the distribution of nodes and members. The truss was modeled using 21 displacement DOFs, with two displacement DOFs in the horizontal and vertical directions at each node, excluding the boundary conditions at both ends. The upper and lower chords of the truss and diagonal members had lengths of 4 and 5 m, respectively, and the vertical members each had a length of 3 m. The modulus of elasticity of the truss members was 200 GPa, and the cross-sectional area was appropriately defined as 5500 mm². The optimal sensor locations were determined by targeting the first six mode shapes.
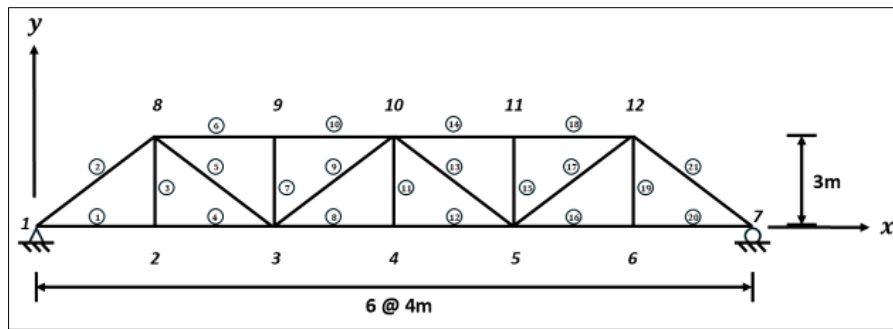
Figure 2. A simply supported truss structure for a numerical example. The circle numbers indicate the member number

In this numerical experiment, six target sensors were employed to track OSP using the first six mode shapes. Initially, the DOF at node 2 in the horizontal direction 2x was regarded as having low independence and was thus designated as a slave DOF. During the iterative process, the proposed objective functions were evaluated at each step to relocate one master DOF to a slave DOF. This process was repeated until the number of candidate sensors matched the number of target sensors.

Figure 3 showcases the final sensor configurations determined by the five proposed algorithms: EI-M1, EI-M2, MMSE, MMAC, and the combined approach (CA). All methodologies integrated constraints based on modal reduction, yet the resultant sensor layouts differed due to variations in objective functions and methodologies. The EI-based methods consistently placed sensors across the span of the truss focusing on high-signal-strength regions while ensuring coverage across the structure. MMSE and MMAC-based approaches prioritized symmetrical sensor placements with higher strain energy or improved modal consistency. The CA method balanced the strengths of MMSE and MMAC, demonstrating versatility for varied structural objectives. The differences in sensor layouts are attributed to the distinct objective functions used in each technique. EI methods aim for independence and uniformity, while MMSE emphasizes areas with high modal energy for damage sensitivity.
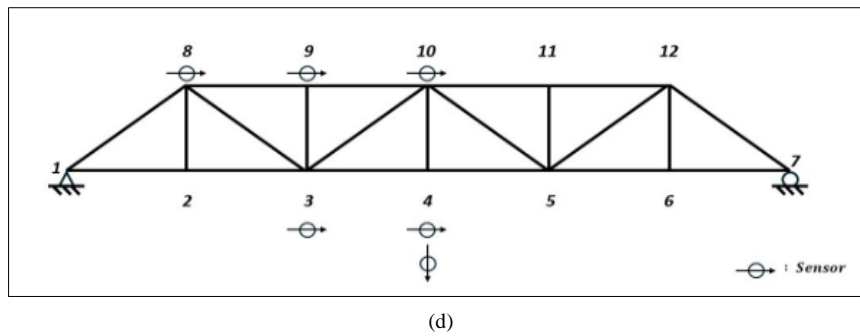

(a)

(b)

(c)

(d)
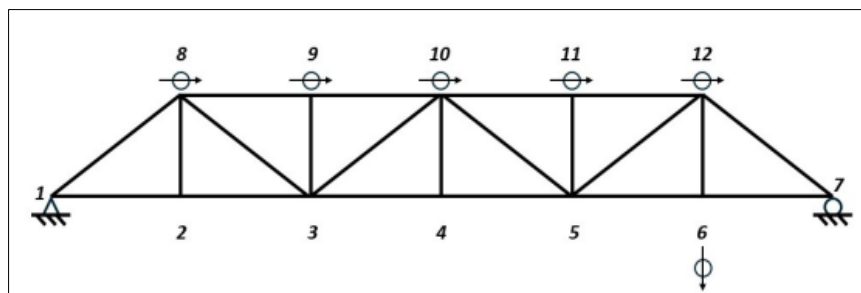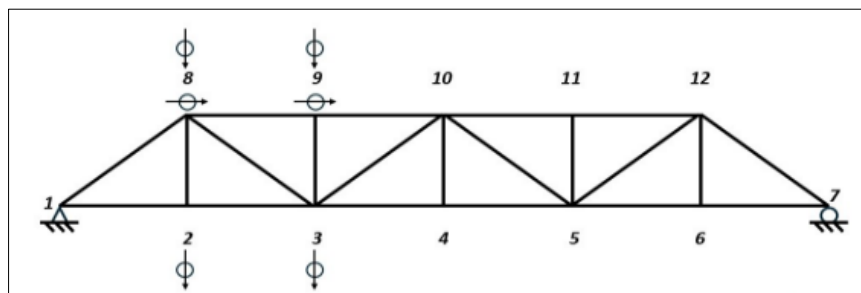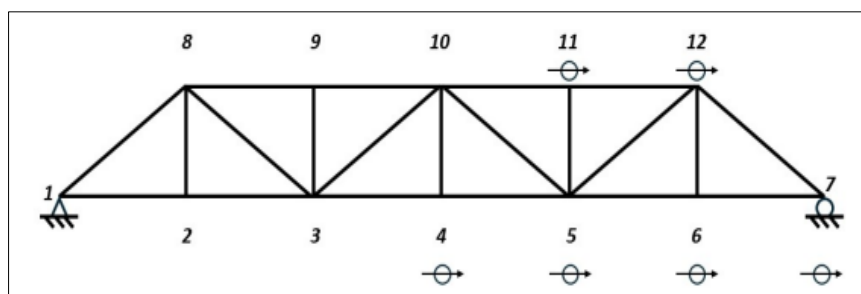
Figure 3. Final sensor designs by the proposed algorithms: (a) EI − M1 and EI − M2, (b) MMSE , (c) MMAC, (d) CA

The iteration routes for these methods, as presented in Table 1, highlight the distinct paths each algorithm takes to achieve the final sensor layouts. The results underscore the influence of objective functions, with EI methods emphasizing uniformity and independence, while MMSE and MMAC prioritize specific high-energy or symmetry-related criteria.

Table 1. Iteration route for the OSP according to the proposed algorithms

Algorithm	Iteration process
EI-M1 and EI-M2	$2x \rightarrow 12y \rightarrow 11y \rightarrow 10y \rightarrow 9y \rightarrow 8y \rightarrow 11x \rightarrow 6x \rightarrow 5x \rightarrow 4x \rightarrow 3x \rightarrow 3y \rightarrow 2y \rightarrow 5y \rightarrow 6y$
MMSE	$2x \rightarrow 11x \rightarrow 5x \rightarrow 4x \rightarrow 12x \rightarrow 6x \rightarrow 10x \rightarrow 7x \rightarrow 3x \rightarrow 11y \rightarrow 5y \rightarrow 6y \rightarrow 12y \rightarrow 10y \rightarrow 4y$
MMAC	$2x \rightarrow 12y \rightarrow 11y \rightarrow 10y \rightarrow 9y \rightarrow 8y \rightarrow 7x \rightarrow 6x \rightarrow 5x \rightarrow 4x \rightarrow 3x \rightarrow 3y \rightarrow 2y \rightarrow 4y \rightarrow 5y$
CA	$2x \rightarrow 12y \rightarrow 6y \rightarrow 8y \rightarrow 2y \rightarrow 4y \rightarrow 11x \rightarrow 5x \rightarrow 11y \rightarrow 5x \rightarrow 11x \rightarrow 12x \rightarrow 6x \rightarrow 7x \rightarrow 10y$

* The number indicates the node number, and x and y are the displacement DOFs in the horizontal and vertical directions, respectively.

The study highlights the strengths of integrating modal reduction constraints and the adaptability of hybrid OSP algorithms. The comprehensive numerical validations provide robust evidence supporting the efficiency and practicality of these methods in SHM applications. Future extensions could include validations under more complex and diverse structural scenarios, enhancing the generalizability of the findings.

The study provides a comprehensive evaluation of OSP algorithms, illustrating their strengths and trade-offs through analytical and numerical comparisons. These findings set a foundation for further refinement and application in real-world SHM systems, where adaptability and efficiency are critical. The study effectively tackles significant challenges in sensor layout design by introducing modified and hybrid OSP algorithms, which address issues such as efficiency, accuracy, and adaptability in SHM.

The analytical and numerical comparisons in the study provide convincing evidence to support the performance of the proposed OSP algorithms. The combination of rigorous theoretical validation and practical numerical experiments demonstrates the algorithms' effectiveness, adaptability, and alignment with SHM objectives. While the results are compelling, further validation across diverse and complex scenarios could enhance the robustness of the findings.

The study provides a strong foundation for reproducibility through detailed descriptions of numerical examples, mathematical formulations, and iterative procedures. However, explicit details about computational tools, boundary conditions, and parameter sensitivities could further enhance reproducibility. With minor additions, the results could be confidently replicated in similar experimental and analytical setups.

4. Conclusion

This study introduces advanced methodologies for OSP in SHM, addressing efficiency and reliability in sensor layout design. By integrating modal reduction constraints with innovative analytical frameworks, the research offers iterative algorithms that maintain high signal fidelity while meeting the constraints of limited sensor deployment. Hybrid methodologies combining MSE, MAC, and EI ensure balanced optimization between data capture and computational efficiency.

The study emphasizes the importance of aligning sensor layouts with specific structural and monitoring objectives. Modal reduction constraints enable meaningful contributions from excluded DOFs in iterative processes, enhancing the accuracy of sensor placement. Numerical validations demonstrate the adaptability of these approaches, yielding configurations tailored to varying performance criteria. The proposed methodologies have broad implications, especially in cost-sensitive or resource-constrained SHM applications. By leveraging hybrid frameworks, stakeholders can achieve effective monitoring with minimal resources. The integration of MSE, MAC, and EI techniques establishes a new benchmark for sensor optimization, facilitating the development of SHM systems for complex infrastructures such as bridges, skyscrapers, and aerospace structures. Validation through numerical experiments, including a simply supported truss structure, confirms the robustness and versatility of these approaches.

Future research could extend this work by exploring real-time adaptive algorithms, integrating machine learning, addressing nonlinear dynamics, and validating the methodologies in real-world scenarios. By harmonizing theoretical innovation with practical applications, this research lays a solid foundation for future advancements in sensor deployment strategies.

5. Declarations

5.1. Author Contributions

Conceptualization, H.C.E., J.Y.K. and J.H.A.; methodology, H.C.E., J.Y.K. and J.H.A.; software, J.Y.K.; writing—original draft preparation, H.C.E.; writing—review and editing, H.C.E., J.Y.K. and J.H.A. All authors have read and agreed to the published version of the manuscript.

5.2. Data Availability Statement

The data presented in this study are available in the article.

5.3. Funding

5.4. Conflicts of Interest

The authors declare no conflict of interest.

6. References

[1] Chen, B., Huang, Z., Zheng, D., & Zhong, L. (2017). A hybrid method of optimal sensor placement for dynamic response monitoring of hydro-structures. International Journal of Distributed Sensor Networks, 13(5), 1550147717707728. doi:10.1177/1550147717707728.

[2] Shi, Q., Wang, X., Chen, W., & Hu, K. (2020). Optimal Sensor Placement Method Considering the Importance of Structural Performance Degradation for the Allowable Loadings for Damage Identification. Applied Mathematical Modelling, 86, 384–403. doi:10.1016/j.apm.2020.05.021.

[3] Tan, Y., & Zhang, L. (2020). Computational methodologies for optimal sensor placement in structural health monitoring: A review. Structural Health Monitoring, 19(4), 1287–1308. doi:10.1177/1475921719877579.

[4] Błachowski, B., Ostrowski, M., Tauzowski, P., Swiercz, A., & Jankowski, Ł. (2020). Sensor placement for structural damage identification by means of topology optimization. AIP Conference Proceedings, 2239, 20002. doi:10.1063/5.0007817.

[5] Lee, E.-T., & Eun, H.-C. (2021). Optimal sensor placements using modified Fisher information matrix and effective information algorithm. International Journal of Distributed Sensor Networks, 17(6), 155014772110230. doi:10.1177/15501477211023022.

[6] Lee, E. T., & Eun, H. C. (2022). Optimal Sensor Placement in Reduced-Order Models Using Modal Constraint Conditions. Sensors, 22(2). doi:10.3390/s22020589.

[7] Gomes, G. F., de Almeida, F. A., da Silva Lopes Alexandrino, P., da Cunha, S. S., de Sousa, B. S., & Ancelotti, A. C. (2019). A multiobjective sensor placement optimization for SHM systems considering Fisher information matrix and mode shape interpolation. Engineering with Computers, 35(2), 519–535. doi:10.1007/s00366-018-0613-7.

[8] Sun, H., & Büyüköztürk, O. (2015). Optimal sensor placement in structural health monitoring using discrete optimization. Smart Materials and Structures, 24(12), 125034. doi:10.1088/0964-1726/24/12/125034.

[9] Kammer, D. C. (1991). Sensor placement for on-orbit modal identification and correlation of large space structures. Journal of Guidance, Control, and Dynamics, 14(2), 251–259. doi:10.2514/3.20635.

[10] Friswell, M. I., & Castro-Triguero, R. (2015). Clustering of sensor locations using the effective independence method. AIAA Journal, 53(5), 1388–1390. doi:10.2514/1.J053503.

[11] Castro-Triguero, R., Murugan, S., Friswell, M.I., & Gallego, R. (2013). Optimal Sensor Placement for Structures Under Parametric Uncertainty. Topics in Dynamics of Bridges, Volume 3. Conference Proceedings of the Society for Experimental Mechanics Series. Springer, New York, United States. doi:10.1007/978-1-4614-6519-5_14.

[12] Gonen, S., Demirlioglu, K., & Erduran, E. (2023). Optimal sensor placement for structural parameter identification of bridges with modeling uncertainties. Engineering Structures, 292(1), 116561. doi:10.1016/j.engstruct.2023.116561.

[13] Penny, J. E. T., Friswell, M. I., & Garvey, S. D. (1994). Automatic choice of measurement locations for dynamic testing. AIAA Journal, 32(2), 407–414. doi:10.2514/3.11998.

[14] Lu, L. L., Wang, X., & Huang, C. G. (2013). A new method of optimal sensor placement for modal identification of offshore platform structure. Proceedings of the 2013 World Congress on Advances in Structural Engineering and Mechanics, 8-12 September, 2013, Jeju, Korea.

[15] Mercer, J. F., Aglietti, G. S., & Kiley, A. M. (2016). Model reduction and sensor placement methods for finite element model correlation. AIAA Journal, 54(12), 3941–3955. doi:10.2514/1.J054976.

[16] He, C., Xing, J., Li, J., Yang, Q., Wang, R., & Zhang, X. (2015). A new optimal sensor placement strategy based on modified modal assurance criterion and improved adaptive genetic algorithm for structural health monitoring. Mathematical Problems in Engineering, 2015. doi:10.1155/2015/626342.

[17] Fu, Y., & Yu, L. (2012). Optimal sensor placement based on MAC and SPGA algorithms. Advanced Materials Research, 594–597, 1118–1122. doi:10.4028/www.scientific.net/AMR.594-597.1118.

[18] Brehm, M., Zabel, V., & Bucher, C. (2010). An automatic mode pairing strategy using an enhanced modal assurance criterion based on modal strain energies. Journal of Sound and Vibration, 329(25), 5375–5392. doi:10.1016/j.jsv.2010.07.006.

[19] Coote, J. E., Lieven, N. A. J., & Skingle, G. W. (2005). Sensor placement optimisation for modal testing of a helicopter fuselage. Proceedings of the 24th International Modal Analysis Conference (IMAC-XXIII), 30 January - 2 February, St. Louis, United States.

[20] Cha, Y. J., & Buyukozturk, O. (2015). Structural damage detection using modal strain energy and hybrid multiobjective optimization. Computer-Aided Civil and Infrastructure Engineering, 30(5), 347–358. doi:10.1111/mice.12122.

[21] Hu, H., & Wu, C. (2009). Development of scanning damage index for the damage detection of plate structures using modal strain energy method. Mechanical Systems and Signal Processing, 23(2), 274–287. doi:10.1016/j.ymssp.2008.05.001.

[22] Shi, Z. Y., Law, S. S., & Zhang, L. M. (1998). Structural damage localization from modal strain energy change. Journal of Sound and Vibration, 218(5), 825–844. doi:10.1006/jsvi.1998.1878.

[23] Seyedpoor, S. M. (2012). A two stage method for structural damage detection using a modal strain energy based index and particle swarm optimization. International Journal of Non-Linear Mechanics, 47(1), 1–8. doi:10.1016/j.ijnonlinmec.2011.07.011.

[24] Pal, J., & Banerjee, S. (2015). A combined modal strain energy and particle swarm optimization for health monitoring of structures. Journal of Civil Structural Health Monitoring, 5(4), 353–363. doi:10.1007/s13349-015-0106-y.

[25] Zhang, Z., Peng, C., Wang, G., Ju, Z., & Ma, L. (2023). Optimal sensor placement for strain sensing of a beam of high-speed EMU. Journal of Sound and Vibration, 542(6), 117359. doi:10.1016/j.jsv.2022.117359.

[26] Liu, W., Gao, W., Sun, Y., & Xu, M. (2008). Optimal sensor placement for spatial lattice structure based on genetic algorithms. Journal of Sound and Vibration, 317(1–2), 175–189. doi:10.1016/j.jsv.2008.03.026.

[27] Zheng, H., Yan, Q., Hu, J., & Chen, Z. (2012). Optimal sensors placement based on modal strain energy. Applied Mechanics and Materials, 166–169, 1164–1169. doi:10.4028/www.scientific.net/AMM.166-169.1164.

[28] Seyedpoor, S. M., Yahyapour, R., Mofdi, A. A., & Fallahian, S. (2024). Structural damage identification through an optimal sensor placement approach and the modal strain energy-based index. Journal of Rehabilitation in Civil Engineering, 12(1), 126-143. doi:10.22075/JRCE.2023.29823.1805.

[29] Salama, M., Rose, T., & Garba, J. (1987). Optimal placement of excitations and sensors for verification of large dynamical systems. Proceedings of the 28th Structures. Structural Dynamics, and Materials Conference. doi:10.2514/6.1987-782.

[30] Li, D. S., Li, H. N., & Fritzen, C. P. (2007). The connection between effective independence and modal kinetic energy methods for sensor placement. Journal of Sound and Vibration, 305(4–5), 945–955. doi:10.1016/j.jsv.2007.05.004.

[31] Nicoletti, V., Quarchioni, S., Amico, L., & Gara, F. (2024). Assessment of different optimal sensor placement methods for dynamic monitoring of civil structures and infrastructures. Structure and Infrastructure Engineering, 1-16. doi:10.1080/15732479.2024.2383299.

[32] Wang, Y., Chen, Y., Yao, Y., & Ou, J. (2023). Advancements in Optimal Sensor Placement for Enhanced Structural Health Monitoring: Current Insights and Future Prospects. Buildings, 13(12), 3129. doi:10.3390/buildings13123129.

[33] Hassani, S., & Dackermann, U. (2023). A Systematic Review of Optimization Algorithms for Structural Health Monitoring and Optimal Sensor Placement. Sensors, 23(6), 3293. doi:10.3390/s23063293.

[34] Mghazli, M.O., Zoubir, Z., Elmankibi, M., & Lamdouar, N. (2024). Comparison of Optimal Sensor Placement Technics for Structural Health Monitoring Application. Proceedings of 5th International Conference on Civil Engineering and Architecture. ICCEA 2022. Lecture Notes in Civil Engineering, 369, Springer, Singapore. doi:10.1007/978-981-99-4049-3_38.

[35] Fan, X. (2021). Advances in Optimal Sensor Placement for Structural Health Monitoring. 2021 4th International Symposium on Traffic Transportation and Civil Architecture (ISTTCA), 12-14 November, 2021, Suzhou, China.

[36] Tang, K., Xu, S., Yang, Y., Kong, H., & Ma, Y. (2024). Optimal Sensor Placement Using Combinations of Hybrid Measurements for Source Localization. 2024 IEEE Radar Conference (RadarConf24), 1–6. doi:10.1109/radarconf2458775.2024.10548509.

[37] Saeed, S., Sajid, S. H., & Chouinard, L. (2024). Optimal Sensor Placement for Enhanced Efficiency in Structural Health Monitoring of Medium-Rise Buildings. Sensors, 24(17), 5687. doi:10.3390/s24175687.